Catal Lett (2008) 122:183–187
DOI 10.1007/s10562-007-9367-3

The Influence of Rh Addition on the Catalytic Activity of Cubic Pt Nanocrystals Supported on Alumina for NO/CH_4 Reaction

Ioan Balint · Akane Miyazaki

Received: 24 October 2007 / Accepted: 23 November 2007 / Published online: 13 December 2007

Abstract The effect of the Rh addition to the well defined cubic (≈70%) Pt nanocrystals of around 13 nm supported on alumina was investigated for NO/CH_4 reaction. The impact of size and shape of Pt nanoparticles on the catalytic activity were also analyzed by comparing the results with a conventionally prepared catalyst.

Keywords Platinum nanoparticles · Rhodium · deNOx catalysts · Methane oxidative conversion

1 Introduction

The catalytic removal of NO from different polluting sources by using hydrocarbon reductants became already a standard procedure for environmental protection. Methane is a convenient reductant because is relatively cheap but on the other hand is the least reactive among hydrocarbons. Under near stoichiometric or methane-rich conditions, platinum has been found to be the most active and stable catalyst [1] but gives relatively high selectivity to harmful products such as N_2O and NH_3. The NO reduction is a structure sensitive reaction [2], depending on the morphology of the supported metal particles. Recently, interesting morphological effects have been revealed by using well-defined Pt nanocrystals [3–5].

The aim of the present work was to investigate the effect of Rh addition on the catalytic behavior of the well-structured (cubic) Pt nanocrystals supported on alumina for NO/CH_4 reaction in methane-rich conditions. The purpose was to improve the selectivity to N_2 without affecting the high catalytic activity of platinum. Another aim was to determine the intrinsic catalytic activity of Pt and Rh-added Pt nanoparticles (expressed as turnover frequency) as well as the associated activation energies for NO/CH_4 reaction.

2 Experimental

The synthesis method of the alumina supported Pt nanoparticles was already reported [4, 5]. The K_2PtCl_4 complex (10^{-4} M aqueous solution) was reduced with H_2 at 40 °C in the presence of NIPA (N-isopropylacryl amide) capping polymer. The resulted Pt nanocrystals of around 13 nm and having mainly cubic shape (≈70%) were supported on γ-Al_2O_3 (Aerosil, 100 m^2 g^{-1}) to get a final metal loading of 1 wt%. After water elimination by freeze-drying the material was calcined air at 350 °C for 1 h to remove the capping polymer. This catalyst will be called hereafter Pt(NIPA). The Rh-added catalyst was prepared by impregnation of Pt(NIPA) with appropriate amounts of $Rh_3(CO)_{12}$ dissolved in tetrahydrofuran. After the solvent removal, the catalyst was calcined again in air at 350 °C for 1 h. The final metal loadings were 0.2 wt% Rh and 1 wt% Pt, hereafter called Pt(NIPA)-Rh. The activities of the Pt(NIPA) and Pt(NIPA)-Rh catalysts were compared with that of a commercial catalyst supplied by Engelhard Corporation Japan, hereafter called Pt(Engel).

I. Balint (✉)
Institute of Physical Chemistry of Romanian Academy, Spl. Independentei 202, 060021 Bucharest, Romania
e-mail: ibalint@chimfiz.icf.ro

A. Miyazaki
Department of Chemical and Biological Sciences, Faculty of Science, Japan Women's University, 2-8-1, Mejirodai, Bunkyo-ku 112-8681, Japan
e-mail: miyazakia@fc.jwu.ac.jp

The catalytic activity was tested in flow system by using a quartz reactor loaded with 0.05 g of catalyst. The flow rate of the reactant mixture (1% NO, 0.4% CH_4 and balance Ar) was 50 cm^3 min^{-1}. The corresponding GHSV (Gas Hour Space Velocity) was 60, 000 h^{-1}.

The samples were characterized by transmission electron microscopy (TEM, Hitachi H-8100); X-ray diffraction (XRD, Rigaku Multiflex difractometer); N_2 adsorption (physical surface); and CO chemisorption (metal surface, Chembet-3000 Quantachrome).

3 Results

Figure 1 presents the TEM images of the cubic ($\approx$70%) Pt nanoparticles of around 13 nm in colloidal stage (a) and after deposition on alumina (b). The high-resolution TEM revealed that the crystallographic orientation of the cubic Pt nanocrystals facets was {100} because the interplanar distance was 0.196 nm. The Rh presence at Pt(NIPA)-Rh catalyst could not be visually evidenced by TEM (see 1c).

The characterization data for the supported Pt catalysts are presented in Table 1. The Pt particles of Pt(Engel) catalyst were too small to be characterized by TEM. The CO chemisorption measurements confirmed the small size of the Pt particles for Pt(Engel) (d_{CO} = 3 nm). In contrast, the average Pt particle size for Pt(NIPA) and Pt(NIPA)-Rh catalysts were significantly larger (d_{TEM} = 13 nm for both catalysts). The average d_{CO} value for the Pt particles of Pt(NIPA) was $\approx$28 nm. The discrepancy between TEM and chemisorption results can be attributed to several factors such as metal-support interaction, variable CO adsorption stoichiometry with metal particle size, etc. [6, 7] The d_{CO} value is not relevant for Pt(NIPA)-Rh catalyst because CO is chemisorbed on the exposed metal sites of Pt as well as of Rh. However, the chemisorption data is useful as site counter used for the calculation of TOF values.

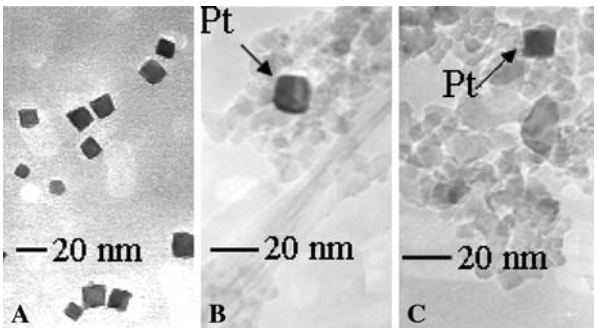

Fig. 1 The TEM micrographs of the cubic colloidal Pt nanoparticles (**a**); (**b**) alumina-supported cubic Pt nanoparticle for Pt(NIPA) catalyst; (**c**) alumina supported metal nanoparticle for Pt(NIPA)-Rh catalyst

Table 1 Characterization data for the alumina-supported Pt particles.

Catalyst	Pt(NIPA)	Pt(NIPA)-Rh	Pt(Engel)
S_{BET} (m^2 g^{-1})	95	88	114
d_{TEM} (nm)[a]	13	13	–
d_{CO} (nm)[b]	28	–	3
Dispersion (%)	3.9	–	38
Exposed metal atoms (μmol g^{-1}catalyst)	1.98	2.9	19.57

[a] The average size was determined from TEM micrographs by counting more than 200 Pt nanoparticles

[b] Average particle size determined from CO chemisorption data

The next step was to compare the catalytic behavior of Pt(NIPA), Pt(NIPA)-Rh and Pt(Engel) for NO/CH_4 reaction. The order of the catalytic activity for the conversions of CH_4 and NO was Pt(Engel) $\geq$ Pt(NIPA)-Rh $\gg$ Pt(NIPA) (see Fig. 2a, b). In great lines, the activity for NO conversion was related to that for methane oxidative conversion. One of the positive effects of Rh addition was to significantly enhance the activity of Pt(NIPA), decreasing the reaction temperature for similar conversion with around 50 °C. From catalytic activity point of view, Pt(NIPA)-Rh resembled more to that of Pt(Engel). The distribution of the reaction products is comparatively presented in Fig. 3. The observed differences can be ascribed to (I) the morphological effects of the Pt particles on the catalytic reaction and to (II) Rh addition.

One of the most important factors is the selectivity to N_2. As can be seen in Fig. 3, low reaction selectivity to N_2 was observed for Pt nanocrystals (the average N_2/N_2O value was $\approx$0.6) as compared to Pt(Engel) (N_2/N_2O at 300, 350 and 400 °C were 0.6, 5.6, and 73.6, respectively). The addition of Rh to Pt(NIPA) significantly enhanced the reaction selectivity to N_2 (close to 100%).

Another point of interest is the production of harmful products, NH_3 and CO. As can be seen in Fig. 3, ammonia formation over the small Pt particles of Pt(Engel) was favored at $T \geq 350$ °C. In contrast, the formation of NH_3 over Pt(NIPA) as well as Pt(NIPA)-Rh was not observed. Small amounts of CO [S(CO) $\approx$ 18%] were observed at 400 °C over Pt(NIPA)-Rh and Pt(Engel) whereas methane was selectively oxidized to CO_2 over Pt(NIPA). The Rh promotion of Pt(Engel) is not as effective as compared to Pt(NIPA) catalyst. Only a slight decrease in NH_3 formation along with the enhancement of CO production was observed in the case of Pt(Engel)-Rh (not shown in Fig. 3). The catalytic behavior of Rh–Pt(Engel) resembles more with that of Rh/Al_2O_3 catalyst, which is a typical partial oxidation catalyst.

The TOF values for CH_4 and NO conversion as a function of reaction temperature are represented in Fig. 4. The well dispersed Pt particles of Pt(Engel) were active to

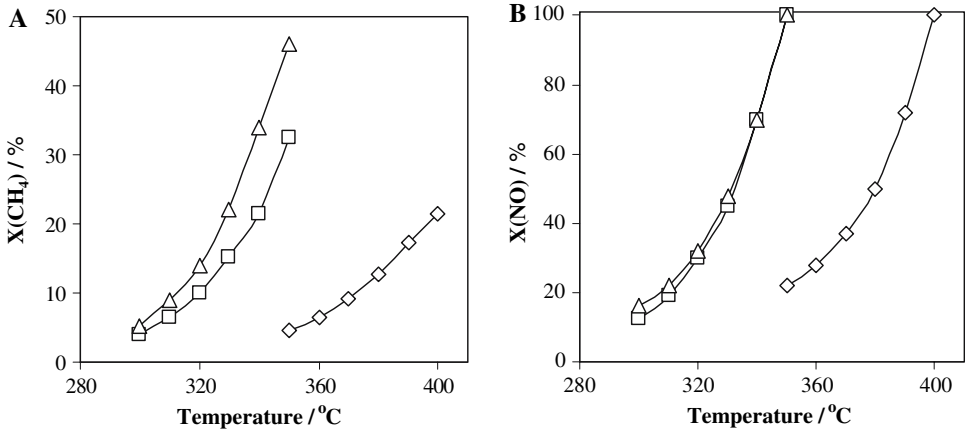

Fig. 2 Comparative methane (**a**) and NO (**b**) conversions over Pt(NIPA) (◇), Pt(NIPA)-Rh (□) and Pt(Engel) (△) catalysts

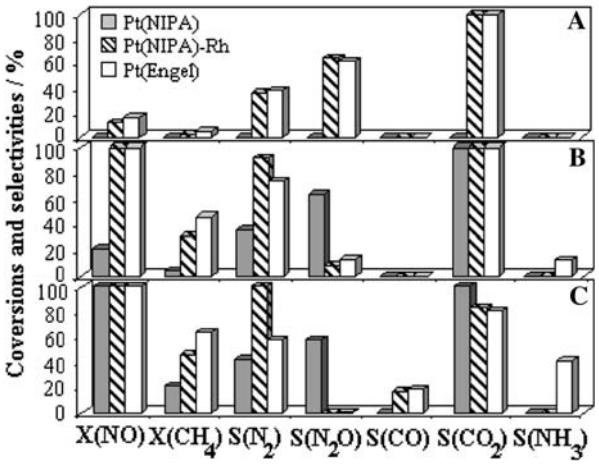

Fig. 3 Comparative conversion and selectivity to products for NO and CH_4 reaction over alumina supported platinum catalysts at 300, 350, and 400 °C

initiate methane activation at lower temperatures but the TOF values were low, increasing progressively with temperature from 0.01 to 0.09. The order of magnitudes for TOF_{CH_4} and TOF_{NO} conversions correlates well with the values reported in literature [1, 8]. The activation temperature for CH_4 over the large metal nanoparticles of Pt(NIPA) was shifted with ≈50 °C to higher values compared to Pt(Engel). Interestingly, the increasing trend of TOF_{CH_4} with temperature for Pt(NIPA) is similar to Pt(Engel). The overlapping of TOF_{CH_4} values for Pt(NIPA) and Pt(Engel) at 350 °C (see Fig. 4a) indicates that the specific activity of surface Pt atoms for methane oxidation not structure sensitive [9]. The TOF values for Pt(NIPA)-Rh were shifted to higher values in the same temperature domain as compared with the Pt(NIPA) and Pt(Engel) catalysts. The experimentally measured overall TOF values contained the specific contributions of both, Pt and Rh sites. The TOF_{CH_4} values for Pt(NIPA)-Rh increased with temperature from 0.04 to 0.039 s^{-1}. The TOF_{NO} values for all the catalysts investigated are with one order of magnitude higher as compared to TOF_{CH_4}, ranging between 0.06 and 3.75 s^{-1}.

The Arrhenius plots for CH_4 and NO reactions are presented in Fig. 5a and b, respectively. The values of the apparent activation energies for CH_4 over the three catalysts investigated were close each other, ranging between 115 and 125 kJ mol^{-1}. Apparent activation energies ranging between 75 and 121 kJ mol^{-1} have been reported for methane combustion over conventional Pt/Al_2O_3 catalysts [8, 9]. The close values of the apparent activation energies suggest a similar reaction mechanism for methane oxidation over the three catalysts investigated. As NO conversion was related to that of CH_4. The apparent activation energies for NO conversion ranged between 109 and 127 kJ mol^{-1}.

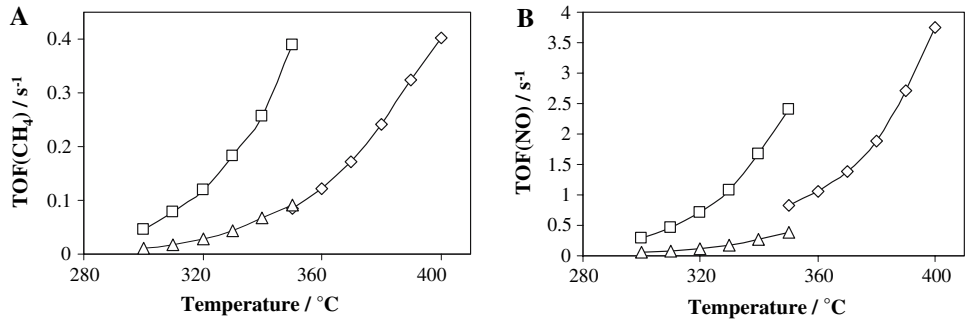

Fig. 4 The dependence of TOF_{CH_4} (**a**) and TOF_{NO} (**b**) on temperature for Pt(NIPA) (◇), Pt(NIPA)-Rh (□), and Pt(Engel) (△) catalysts

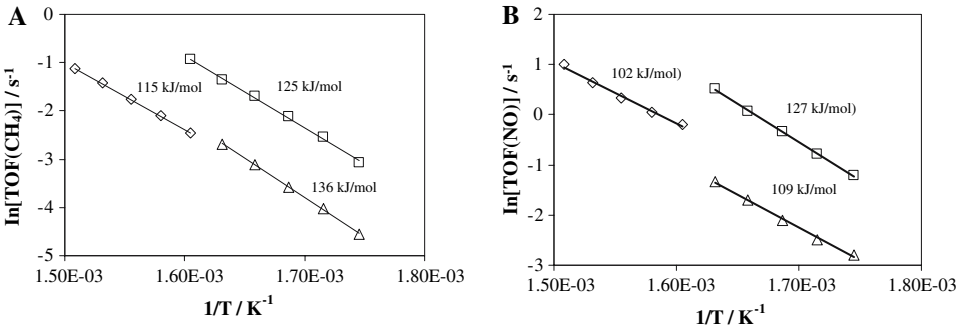

Fig. 5 The Arrhenius plots for CH_4 (**a**) and NO (**b**) conversion rates for Pt(NIPA) (◇), Pt(NIPA)-Rh (□), and Pt(Engel) (△) catalysts

4 Discussion

The NO reduction was selected as test reaction because the making of N–N bond is structure sensitive [2]. Therefore, a suitable morphological control of the supported Pt particles should give useful information regarding the "size" and "shape" effects on their catalytic behavior.

It is accepted that the adsorbed oxidant on the metal surface promotes methane activation [10, 11]. Taking into account the excess methane, it can be assumed that in reaction conditions large portions of Pt surface will be in metallic state and thus available for NO dissociation. Starting from this assumption it is assumed that the information from clean surface studies can be used to explain in a satisfactory manner our experimental results.

The studies performed on the clean surfaces of platinum single crystals point out that the low NO surface coverage ($\Theta < 0.3$), high-index Pt planes (i.e. 410) [12] and high concentration of surface defects, edges, and kinks [13] favor the dissociation of NO into N_{ads} and O_{ads} atoms. There are also consistent proves that N_2 and N_2O are formed via $N_{ads} + N_{ads}$ and $N_{ads} + NO_{ads}$ reactions, respectively [12, 14]. Thus, the catalyst having high activity for NO dissociation should also exhibit high selectivity to N_2. The formation of N_2O was favored over Pt(NIPA) catalyst (see Fig. 3) because of the low activity of the large Pt nanocrystals for NO decomposition. In contrast, the high selectivity to N_2 observed over Pt(Engel) can be explained by the high efficiency of the small polycrystalline Pt particles to decompose NO. The addition of Rh to the Pt(NIPA) catalyst had a beneficial effect by enhancing the catalytic activity for methane conversion and by significantly increasing the reaction selectivity to N_2. The explanation resides in the fact that NO reduction over Rh-based catalysts yields selectively N_2 [1].

The apparent activation energies of methane were close each other, ranging between 115 and 136 kJ mol^{-1} (see Fig. 5a). These experimental values, close to the energy required for methane dissociation (121 kJ mol^{-1}), are in agreement with most of studies suggesting that the rate-determining step is methane activation [15]. The nature of adsorbed oxygen is dependent on the platinum morphology [16, 17]. The TOF values calculated for the large Pt particles are at least one order of magnitude higher than those found for the well-dispersed Pt particles [18, 19]. Thus, CH_4 was selectively oxidized over Pt(NIPA) catalyst by the O_{ads} resulted from NO decomposition to CO_2. The small Pt particles can be easier converted in reaction condition to PtO_x species which can further interact with the support to give $PtAl_xO_y$ species [18]. Because of the low oxidation ability of PtO_x and $PtAl_xO_y$ species, some of the surface carbonaceous species will undergo only to a partial oxidation to give CO.

The relative large amounts of NH_3 were formed over the conventional Pt(Engel) can be explained also by the low oxidation ability of PtO_x species, favoring the

$$CH_x + N_{ads} \rightarrow NH_3 \text{ and } H_{ads} + N_{ads} \rightarrow NH_3$$

reactions. The formation of NH_3 over Pt(NIPA) and Pt(NIPA)-Rh was prevented because the active oxygen chemisorbed on the large Pt particles and rhodium sites rapidly removes the carbonaceous and H species from the catalyst surface as CO_2 and H_2O. One of the effects of Rh addition to Pt(NIPA) was to trigger the formation of small amounts of CO (Fig. 3c). It is well known that Rh-based materials are effective catalysts for partial oxidation of methane to CO and H_2. At higher reaction temperatures, Pt(NIPA)-Rh start to exhibit features which are characteristic for partial oxidation catalysts.

The Pt(NIPA)-Rh catalyst showed a stable activity during 180 h time on stream at 400 °C, the conversions of NO and methane remaining unchanged. Another remarkable feature is that after 65 h of time on stream at 400 °C the selectivity to CO dropped to zero.

5 Conclusions

The NO/CH_4 reaction is structure sensitive, depending both on the size and the shape (facet) of the Pt nanoparticles. The "facet" effect plays an essential role in NO dissociation, thus is responsible for the reaction selectivity to N_2O and N_2. The "size effect" is responsible for the selectivity to CO and NH_3 by controlling the oxygen activity. The Rh

addition to Pt(NIPA) had a positive effect not only by enhancing the selectivity to N_2 but also by increasing the catalyst activity for NO conversion. Over Pt(NIPA)-Rh catalyst the selectivity to N_2O was negligible and the formation of ammonia was completely prevented. The only observed back draw of Rh addition was the formation of small amounts of CO at high reaction temperatures.

Acknowledgment We are grateful to CNCSIS for financial support for this work through the grant no. 724.

References

1. Burch R, Ramli A (1998) Appl Catal B 15:49
2. Gates BC (1995) Chem Rev 95:511
3. Balint I, Miyazaki A, Aika K (2002) Chem Comm 10:1044
4. Miyazaki A, Nakano Y (2000) Langmuir 16:7109
5. Balint I, Miyazaki A (2004) In: Schwarz JA, Contescu C, Putyera K (eds) Encyclopedia of nanoscience and nanotechnology. Marcel Dekker, New York, pp 2259–2268
6. Rickard JM, Genovese L, Moata A, Nitsche S (1990) J Catal 121:141
7. Freel J (1972) J Catal 25:149
8. Garetto F, Apesteguia CR (2000) Catal Today 62:189
9. Burch R, Loader PK (1994) Appl Catal B 5:149
10. Aghalayam P, Park YK, Fernandes N, Papavassiliou V, Mhadeshwar AB, Vlachos DG (2003) J Catal 213:23
11. Burch R, Loader PK (1995) Appl Catal A 122:169
12. Banholzer WF, Masel RI (1984) J Catal 85:127
13. Zambelli T, Wintterlin J, Trost J, Ertl G (1996) Science 273:1688
14. Root TW, Schmidt LD, Fisher GB (1983) Surf Sci 134:30
15. Hickman DA, Schmidt LD (1992) J Catal 138:267
16. Burch R, Hayes MJ (1995) J Mol Catal A 100:13
17. Kneringer G, Netzer FP (1975) Surf Sci 49:125
18. Hicks RF, Qi H, Young ML, Lee RG (1990) J Catal 122:280
19. Labame V, Garbowski E, Guilhaume N, Primet M (1996) Appl Catal A 138:93